A Pocket-Sized 3D-printed Attenuated Total Reflection-Infrared Filtometer combined with Functionalized Silica Films for Nitrate Sensing in Water

Bettina Baumgartner, Stephan Freitag, Christoph Gasser and Bernhard Lendl*

Research Division of Environmental Analytics, Process Analytics and Sensors, Institute of Chemical Technologies and Analytics, Technische Universität Wien, Getreidemarkt 9, 1060 Vienna, Austria

Abstract

Strong anion-exchange materials carry a positive charge that allows them to trap and concentrate anions while releasing other anions. Here, we introduced an ion exchange group into mesoporous silica films coated on attenuated total reflection (ATR) crystals to enrich nitrate from aqueous phase in the volume probed by the evanescent field. The ion-exchange and enrichment capabilities of the films were characterized using standard FTIR spectroscopy. Thereby fast analyte enrichment and full sensor recovery were observed. In addition, high enrichment factors of up to 1600 were achieved. After characterization, these coated ATR crystals were used in a dedicated ATR-IR filtometer comprising a Fabry-Pérot filter detector unit and a miniaturized thermal emitter with a footprint of only 80 mm × 120 mm × 70 mm. The filter covered the spectral region between 1250 - 1800 cm^{-1} allowing for recording IR spectra of nitrate enriched into the mesoporous silica film. The sensor was calibrated using the Langmuir adsorption model as calibration function. From this, a limit of detection of 1.2 mg L^{-1} was derived for the ATR-IR filtometer. This emphasizes the high potential of functionalized mesoporous silica films combined with low-cost filtometers for portable water sensors.

Keywords: Mid-IR Spectroscopy, Mesoporous Materials, Sensing, Ion-Exchange, Functional Coating, Nitrate, 3D-printing

1. Introduction

Safe water supplies are essential for human health and environmental protection. In this context, nitrate is one of the major waterborne chemical hazards and even short term exposure leads to severe health effects.[1] Nitrate concentrations in water supplies scale with human activity particularly due to their intensive use in agriculture and animal breeding.[2] Due to their high water solubility, nitrate eventually find its way into ground water and hence into drinking water supplies.[2,3] Therefore, pollution with nitrate is typically high in rural areas and regularly exceeds the world health organization guideline value of 50 mg L^{-1}. Up to date, nitrate is quantified either spectrophotometrically as nitrite after reduction catalyzed by Cd-salt or enzymes, via ion chromatography, or via ion-selective electrodes.[4] In addition, broad-band ultraviolet/visible spectroscopy-based on-line probes for water monitoring have emerged.[5] These systems have been employed for complex water streams, *e.g.* with high turbidity, relying on sophisticated calibrations dedicated to each application.[5–7] Apart from these established techniques, infrared (IR) spectroscopy provides quantitative chemical information that can be obtained in reagent free measurements in real time. Ions like nitrate show strong and specific bands in the mid-IR spectrum. The asymmetric NO_3 stretching vibration is located at 1395 cm^{-1}. However, quantification of this band in the IR spectrum is made difficult by the strong background absorption of water, which limits the optical path length and hence sensitivity. Attenuated total reflection (ATR) IR spectroscopy is commonly employed for spectroscopic studies of aqueous samples.[8] It was demonstrated that the sensitivity of this technique can be vastly increased using selective enrichment layers coated on ATR crystals that cover the volume probed by the evanescent field.[9–11] Until now, they have been primarily employed for enriching apolar substances into hydrophobic coatings. In this context, we have successfully shown that organically functionalized mesoporous silica films can also be employed.[12] Besides the short response times found for mesoporous silica, their rich surface chemistry allows for tuning their functionality beyond hydrophobicity. The successful nitrate removal of functionalized silica materials with a trimethylammonium-moiety as ion exchange group has been shown for powder materials in batch experiments.[13,14] However, the possibility to fully recover these materials and use them as sensor is still pending. In this work, this question is targeted and a trimethylammonium-moiety was covalently functionalized into a mesoporous silica films coated on ATR crystals. The sensing performance for nitrate in aqueous solutions was studied using a Fourier transform (FT) IR spectrometer.

These spectrometers are still considered as gold-standard for IR spectroscopy. The broad spectral coverage and robustness of FTIR spectrometers enabled applications in a variety of analytical tasks

including quantitative analysis of liquids in off-line as well as in-line applications,[15–20] studying reactions at surfaces,[21–23] as well as clinical diagnositics.[24] An emerging, cost-effective alternative to FTIR spectrometers are filtometers that, in comparison with benchtop spectrometers, allow on-site measurements due to their small size and low energy consumption. In contrast to Michelson interferometers, wavelength discrimination is achieved by the use of optical band pass filters.[25] Based on this principle, Fabry-Pérot (FP) filter designs have emerged in the 1990s that discriminate the transmitted wavelength by the distance *d* between two coplanar reflective surfaces and the refractive index between these surfaces.[26] By changing *d*, the filter can be spectrally tuned and the spectral resolution varies between 20 cm^{-1} up to 50 cm^{-1}, depending on the wavelength range.[27] A micro-electro-mechanical system (MEMS)-based mid IR filter using a FP air resonator combined with a pyroelectric detector was first reported in 2003 and is now commercially distributed in several MIR wavelength ranges.[28,29] FP filter-detectors have been successfully paired with miniaturized pulsed MIR emitters were employed for process gas monitoring in transmission gas cells,[30–32] for liquid sensing,[33] imaging systems[34] as well as paired with a supercontinuum laser for standoff IR spectroscopy.[32] These reports achieved adequate analytical performance without the high spectral resolution and the full spectral coverage provided by FTIR spectrometers while reducing the costs and size of the respective sensing system.

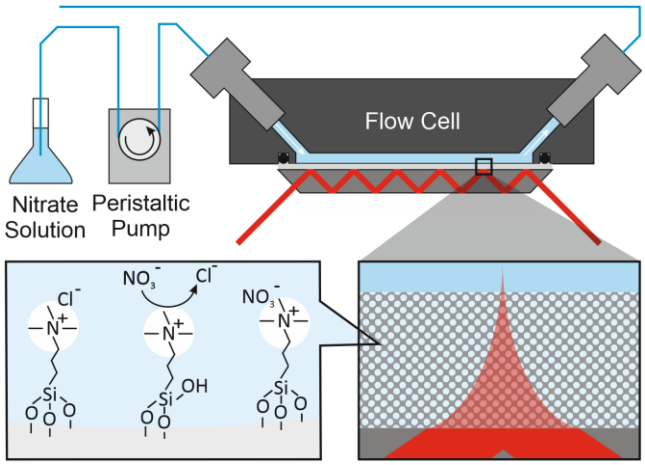

Figure 1: Ge ATR crystal (dark grey) coated with mesoporous silica film functionalized with trimethylammonium moieties allowing for ion-exchange of Cl^- to NO_3^- ions. The coated ATR crystal is placed in a flow cell supplied with nitrate solutions via a peristaltic pump. IR absorbance takes place within the evanescent field (light red), which extends beyond the crystal into the film.

The aim of this contribution is to demonstrate a small, cost-effective mid-IR sensor for nitrate in aqueous solutions based on a 3D-printed ATR-IR filtometer. Germanium ATR crystals coated with a

trimethylammonium-functionalized mesoporous silica films for nitrate sensing were developed (compare Figure 1) and their sensing performance were investigated using FTIR spectroscopy revealing short response times of less than 1 min and high enrichment factors of up to 1600. In a subsequent step the coated ATR crystals were transferred into a dedicated 3D-printed unit comprising light source, FP filter-detector and printed circuit board with a footprint of only 80 mm × 120 mm × 70 mm (compare Figure 2). Although having a lower signal to noise ratio and smaller spectral coverage compared to a FTIR spectrometer, the high enrichment factors of the functionalized ATR crystals allowed for sensing NO_3^- concentrations as low as 3.6 mg L^{-1}. Given the high versatility of silica and low cost of the FP filters, these results demonstrates the high potential of functionalized mesoporous materials in combination with an ATR-IR-filtometer for water monitoring.

2. Materials and Methods

Tetraethoxysilane (TEOS, Sigma Aldrich 99.5%), abs. ethanol (Fisher, 99.6%), hydrochloric acid (VWR, 37%), cetyltrimethylammonium bromide (CTAB, Sigma Aldrich, 99%), N-[3-(trimethoxysilyl) propyl]-N,N,N-trimethylammonium chloride (TMAC, Sigma Aldrich, 50 % in methanol), were used as received. Aqueous $NaNO_3$ solutions were prepared by weight.

2.1. Synthesis of mesoporous films

Mesoporous silica film synthesized using CTAB was prepared as previously reported with a final molar ratio of 1:13:5:5 × 10^{-3}:0.12 for TEOS:EtOH:H_2O:HCl:CTAB.[12] The mixture was stirred for 3 h at 40°C. The film was spin coated with a spinner velocity of 2000 rpm and subsequently calcined at 400 °C for 4 h with a heating ramp of 1 K min^{-1}. For surface functionalization, the coated ATR crystal was placed in a 3-neck flask and 15 mL methanol and 0.5 mL TMAC solution were added. The solution was heated to reflux temperature for 8 h. Subsequently, films were rinsed with acetone and heated to 60 °C in the oven over night.

The characterization of the films using X-ray diffraction and profilometry was performed accordingly to our previous reports.[12,21]

2.2. Optical Setup for FTIR Spectroscopy

Mesoporous silica films were coated on Ge ATR crystals (20 × 10 × 0.5 mm^3) cut from double side polished wafers and polished narrow facets with a defined angle of 45°. This ATR crystal configuration comprises 20 active bounces and a depth of penetration (per bounce) of 420 nm at 1500 cm^{-1} (n_{Ge}=4.02,

n_{sample}=1.33).[8,35,36] The ATR crystals were inserted into a custom-made mount and fixed with a FKM O-ring and an aluminum liquid flow cell with a volume of ca. 20 µL.[12] Two gold mirrors directed the IR beam onto the ATR facet and the detector. The optical setup was placed in the sample compartment of a Vertex 80v FTIR spectrometer (Bruker Optics, Germany) equipped with an N_2-cooled MCT detector. Spectra were recorded with 4 cm^{-1} resolution and 32 scans were averaged per spectrum (double-sided, backward-forward acquisition mode, 8 s per spectrum). Prior to spectrum acquisition, the spectrometer sample compartment was flushed with dry air. The noise floor of the system was obtained by means of 100 % lines, i.e. a scan of the N_2 flushed flow cell with a background scan obtained under same conditions and yielded an RMS noise of $3 \cdot 10^{-5}$ A.U. between 1800 cm^{-1}- 1450 cm^{-1}. Spectra were analyzed using the software package OPUS 7.5 (Bruker Optics, Germany).

2.3. Liquid Handling

Pure water, 0.1 M HCl and nitrate solutions with different concentrations were applied at a flow rate of 1 mL min^{-1} using a peristaltic pump (Ismatec, Germany), and 1/16-in (see Figure 1 for setup). PTFE tubing with 0.5 mm inner diameter was connected to the aluminum flow cell and the peristaltic pump.

2.4. 3D-printed ATR-IR Filtometer

The ATR-IR filtometer was built using a pulsed light source EMIRS200 (Atricle No. 601.612, Reflector 3, CaF_2 window, front-vented, Axetris, Switzerland) a MEMS-based mid-IR filter using a Fabry-Pérot air resonator combined with a pyroelectric dector (LFP-5580C-337, TO8 housing, InfraTec, Germany) covering a spectral range between 1900 cm^{-1}-1250 cm^{-1} and corresponding preamplifier electronics from InfraTec. All parts were integrated in a 3D-printed ATR unit that housed the ATR crystal and defined the angle of incidence for ATR crystal to be 45° (see Figure 2). Ge ATR crystals were used to assure transparence for the mid-IR irradiation in the targeted spectral region between 1250 - 1500 cm^{-1}.

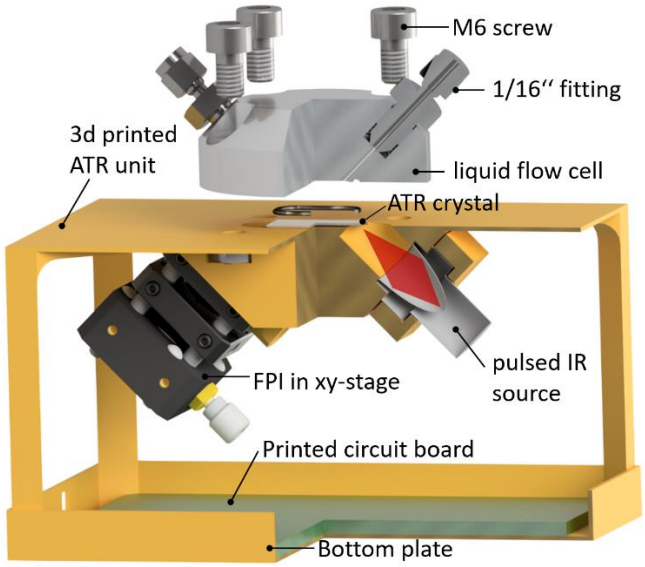

Figure 2: Exploded view of the 3D-printed mini-spectrometer with a footprint of 80 x 120 x 70 mm.

Following the blueprints of the ATR-IR filtometer cartridge developed in Inventor Professional 2017 (Autodesk, USA) the components were sliced using Slic3er Prusa Edition v1.40.1 software (Prusa Re-search, Czech Republic). A Prusa i3 MK3 3D printer (Prusa Re-search, Czech Republic) was used for additive manufacturing. The hotend of the extruder was equipped with a 0.4 mm brass nozzle. PLA with a diameter of 1.75 mm sourced from Prusa (Prusa Re-search, Czech Republic) was printed at 200 °C (First layer 220 °C). The layer height was set to 0.15 mm (0.2 mm for the first layer). Lifting of the Z axis, when filament retraction is triggered was set to zero to avoid stringing, therefore post processing of the printed parts was not requiered. The infill was set to 20 % using a honeycomb pattern. No support structures were used. Further printing parameters were chosen as suggested by Slic3r for Prusa PLA.

The pulsed light source was accommodated in a dedicated, 3D-printed cartridge, which was fixed with two M3 screws and triangular slots without the need of any further optical components. The distance between light source and the facet of the ATR crystal was designed to meet the focal point of the source of 25 mm. On the filter side, a 16 mm cage system (Thorlabs GmbH, Germany) was fixed to the ATR unit with a M2 countersunk screw and the cage system comprised a ZnSe lens (1/2'', F = 12 mm) focusing the MIR beam to the FP filter that was placed in a x-y stage (SCP05, Thorlabs). Strong absorption of PLA of which the ATR unit consist off, was avoided by placing a small piece of glass between ATR crystal and ATR unit. The bottom plate was designed to hold the props of the ATR unit and to house the preamplifier board, which controled source and filter. The board was supplied with 5 V and connected to a PC via USB.

Four M6 nuts were sunk in slits enabling mounting of the liquid flow cell (see section 2.3 further details on the flow cell), which was attached to the peristaltic pump for sample application.

2.4.1. Noise-Characterization of the ATR-IR Filtometer

For characterizing the setup, the light source was operated with different current and the FP filter software was set to different average (= avg) between 1 and 16 data points per wavelength. The noise was derived by means of 100 % lines for different settings and the corresponding spectra are given in Figure 3. The lowest root-mean-square (RMS) noise for the entire spectral region was found to be $2.2 \cdot 10^{-3}$ A.U for a current of 100 mA and maximum averaging of 16 data points per wavelength (avg=16). Therefore, all experiments were performed with these settings. As averaging scales inversely with scanning time, the time needed to record a spectrum with avg = 16 was ca. 2 min.

The single channel spectrum obtained from 100 mA and avg = 16 for a coated Ge ATR crystal is also given in Figure 3 (right y-axis).

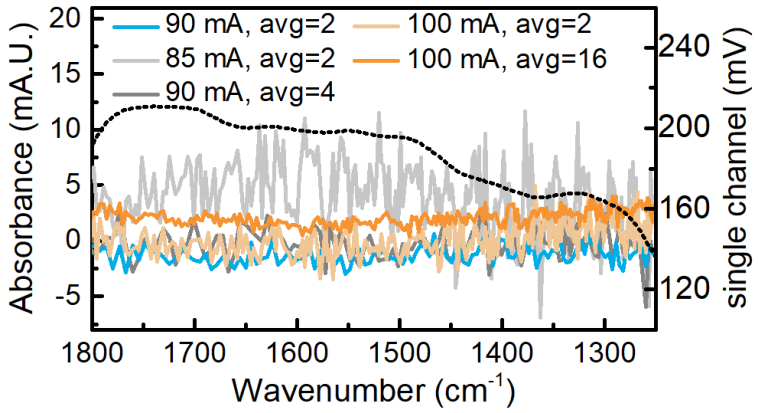

Figure 3: Light source was operated with different current. The corresponding 100 % lines show lower noise levels for higher current. A single channel spectrum of a coated Ge ATR crystal for 100 mA, avg=16 is also given (dotted line, right y-axis)

3. Results and Discussion

3.1. Characterization of Functionalized Mesoporous Films using FTIR spectroscopy

Mesoporous silica films with a pore size of 5 nm were prepared via the evaporation induced self-assembly process using CTAB as template as previously reported.[12,21,37,38] The formation of silica, complete removal of the template and successful surface functionalization was confirmed by FTIR measurements.

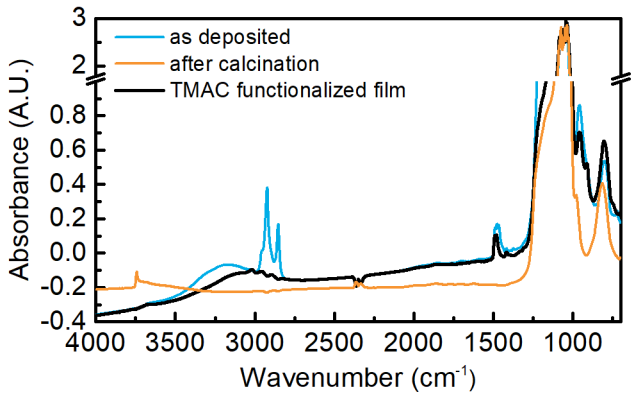

Figure 4: ATR IR spectra of CTAB 3d hexagonal film before calcination, after functionalization with TMAC. Background spectrum was recorded for an uncoated Ge ATR crystal.

The spectra obtained between each step of the synthesis are given in Figure 4. After film deposition and before calcination strong C-H stretching vibrations between 2800 cm^{-1} - 3000 cm^{-1}, the -CH_2 deformation band at 1470 cm^{-1} and the C-N vibration of the trimethylammonium group at 1480 cm^{-1} were visible and correspond to the CTAB template. After calcination, the bands associated with the template had completely vanished and a band at 3745 cm^{-1} corresponding to isolated Si-OH groups arose.[39] In the subsequent step, these groups were saturated with TMAC. The band linked to the trimethylammonium group can be found at 1480 cm^{-1} after functionalization. The presence of this band and the absence of free silanol groups (no band at 3745 cm^{-1} is visible) confirmed the successful functionalization.

3.1.1. FTIR Spectra of Nitrate Enriched into Mesoporous Silica Films

The trimethylammonium functionality is considered a strong anion exchange moiety, thus it demands for a regeneration step. Here, 0.1 M HCl was used as regeneration solvent to yield -$N(CH_3)_3^+Cl$. Spectra of water and 0.1 M HCl applied to the functionalized film were recorded and considerable spectral changes were observed for the O-H stretching and H-O-H bending vibrations at ~ 3400 cm-1 and 1640 cm^{-1}, respectively (see Figure 5).[40,41] A difference spectrum was derived using the spectrum obtained from pure water as background to highlight the differences which are mainly due to the H_3O^+ species present at this low pH.

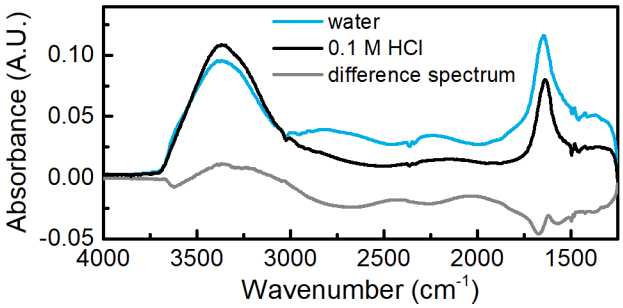

Figure 5: ATR IR spectra recorded after flushing water and 0.1 M HCl for 5 min over a functionalized TMAC CTAB film. Background spectrum was taken for the dry film. The difference spectrum was calculated using the water spectrum as background spectrum.

A shift in the IR spectrum of water arose again upon changing from the regeneration solution back to distilled water. IR spectra for nitrate quantification were calculated using a pure water spectrum as background. An exemplary difference spectrum obtained from the enrichment of a 29 mg L^{-1} NO_3^- solution compared to a reference spectrum is shown in Figure 6. The spectrum is in accordance with the spectrum obtained on a commercial single bounce ATR unit from a 10 g L^{-1} $NaNO_3$ solution. This demonstrates the capability of nitrate sensing using TMAC-functionalized mesoporous silica films. Note that measurements of a 29 mg L^{-1} NO_3^- solution on blank Ge ATR crystals without functionalized mesoporous film did not show spectral features corresponding to NO_3^- as the sensitivity was too low.

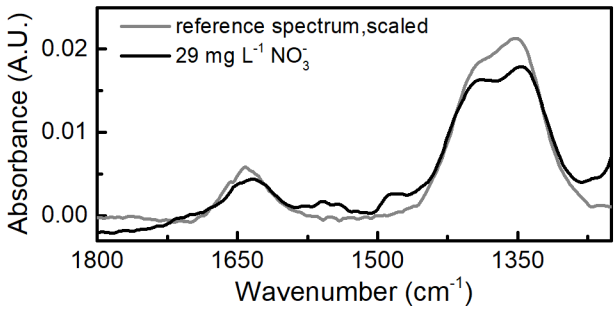

Figure 6: ATR IR spectra of a nitrate enriched in the mesoporous silica film from a 29 mg L^{-1} NO_3^- solution compared with a scaled spectrum of a 10 g L^{-1} $NaNO_3$ solution recorded on a single-bounce ATR unit. Bands corresponding to the NO_3^- stretching mode (1395 cm^{-1} and 1350 cm^{-1}) and H-O-H bending vibration of water (1640 cm^{-1}) are visible.

3.1.2.Monitoring Anion-Exchange using FTIR Spectroscopy

The response time of the TMAC-functionalized mesoporous silica film was determined by exchanging the regeneration solution by nitrate solutions of different concentrations while recording spectra every 4 s. All nitrate enrichment experiments were performed by flushing 5 mL of 0.1 M HCl for conditioning of the

film followed by 5 mL of the respective nitrate solution with 1 mL min^{-1} flow velocity using a peristaltic pump. The nitrate band was integrated between 1465 cm^{-1} and 1290 cm^{-1} and the band areas during application for different nitrate concentrations are given in Figure 7. These profiles show a fast enrichment that stabilizes within the first 100 s. Note that due to the pH dependent changes in the baseline when changing diluted HCl to nitrate solutions, the time profile do not return to 0 but stabilize within 30 s for all concentrations.

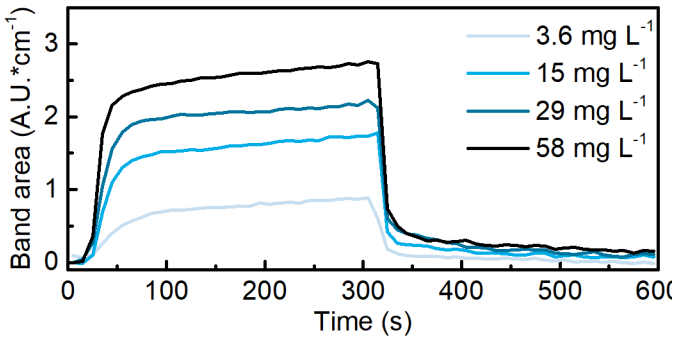

Figure 7: Nitrate band area as function of time for different NO_3^- concentrations. After 300 s of nitrate solution application, regeneration with HCl was performed.

Apart from response times, the concentration of interacting trimethylammonium present in the film could be determined from these measurements: We have recently introduced a method to calculate the effective path length within the film $d_{e,film}$.[12] Here, the effective path length typically used for ATR spectroscopy, is scaled by the finite fraction of the evanescent wave within the film.Based on these calculations, we derived $d_{e,film}$ of the employed 400 nm thick film to be $d_{e,film}$ = 5.71 µm (at 1480 cm^{-1}, n_1=4.02, n_2=1.33).[12,35,36] The absorption coefficient of C-N^+ vibration of the TMAC moiety was retrieved from IR transmission measurements and equals to $\varepsilon(1480\ cm^{-1})$ = 4792 L cm^{-2} mol^{-1} for the band area integrated between 1532 - 1432 cm^{-1}. Inserting into Lambert-Beer's law with $A = \varepsilon \cdot c \cdot d_{e,film}$ yields a trimethylammonium concentration of 0.4 mol L^{-1}_{film}, which is equivalent to $3.5 \cdot 10^{-8}$ mol_{NH3+} per film volume calculated as 20 mm x 10 mm x 400 nm. If assuming that every chloride ion from the regeneration step is replaced with a nitrate ion, this would correspond to a NO_3^- concentration of 24.8 g L^{-1}_{film}. The absorption coefficient of the nitrate band between 1250 cm^{-1} and 1500 cm^{-1} was derived from an IR transmission measurement of a 7.9 g L^{-1} NO_3^-solution to be ε = 698 L g^{-1} cm^{-2}. Based on the same principles, the nitrate concentration in the film obtained from the enrichment experiment of a 3.6 mg L^{-1} NO_3^- solution was calculated to be 1.91 g L^{-1}. This corresponds to trimethylammonium moiety consumption of 8 % and an enrichment factor of 530.

Until now, standard solutions were obtained from $NaNO_3$ dissolved in distilled water. Therefore, no potentially interfering counter ions were present. To account for them, standard solutions were prepared containing 20 mg L^{-1} $NaNO_3$ and 20 mg L^{-1} Na_2SO_4. However, no nitrate enrichment could be achieved, as it seems that the affinity of the trimethylammonium groups was higher toward multiply charged anions such as sulfate.

3.2. Nitrate Sensing using an ATR-IR Filtometer

In contrast to the high-end FTIR spectrometer employed for the film characterization, the RMS noise of the presented ATR-IR filtometer was a factor 100 higher and it also offered a lower spectral resolution. However, due to the high enrichment factor facilitated by the TMAC-functionalized film and the broad absorption band of NO_3^-, quantitative measurements of nitrate concentrations at drinking water levels could be achieved. In contrast to the measurements performed with the FTIR spectrometer, recording of one spectrum (averaging of 16 measurements for each data point, at 10 Hz) takes 2 min. Thus, no time profiles could be retrieved with this setup, but a spectrum after the application of 5 mL NO_3^- solution with 1 mL min^{-1} flow rate was recorded. Spectra obtained for different nitrate concentrations are given in Figure 8A and clearly show that a NO_3^- concentration of 3.6 mg L^{-1} is still detectable. Note that due the instability of the film and leaching of the TMAC moieties out of the film the enrichment capacity of film decreased over time. Spectra given in Figure 8A were recorded directly after film synthesis while the same film was used two weeks later for measurements with the FTIR spectrometer showing already a decreased enrichment capacity. However, repeated measurements without significant decay in performance were feasible. This is reflected in the small error bars given in Figure 8B for three subsequent enrichment experiments.

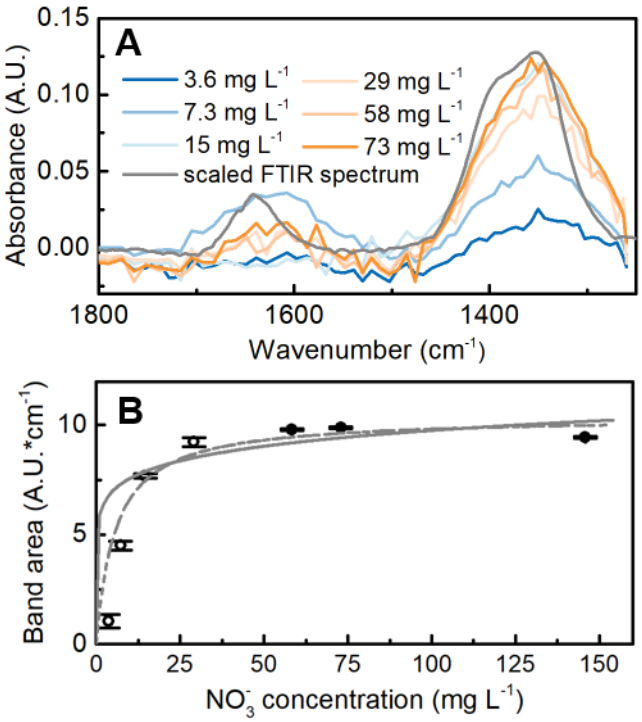

Figure 8: (A) IR spectra obtained with the ATR-IR filtometer for different nitrate concentrations. The background spectrum was recorded with distilled water. (B) Nitrate band area as function of applied concentration. Data points were fitted with the Langmuir function (dashed line) and Freundlich function (solid line).

The obtained band areas for three consecutive adsorption experiments per concentration after 5 min were plotted as function of applied nitrate concentration in Figure Figure 8B. The obtained isotherms were fitted with the Langmuir and the Freundlich functions:

$$q_e = \frac{q_m K_\mathrm{L} c}{1 + \mathrm{K_L} c} \quad (1)$$

$$q_e = K_\mathrm{F} c^{\frac{1}{n_F}} \quad (2)$$

where q_e (A.U. cm^{-1} for data obtained from IR absorption bands) is the amount of adsorbed analyte, q_m (A.U. cm^{-1}) is the maximum adsorption capacity, c is the concentration of applied nitrate solutions (mg L^{-1}), K_L (L g^{-1}) is the Langmuir constant, K_F (A.U. cm^{-1} [g L^{-1}]$^{-1/n}$) is the Freundlich affinity coefficient, and n_F (unitless) is the Freundlich linearity index. In contrast to the adsorption isotherms obtained in our previous report for aliphatic and aromatic nitrile enrichment into hydrophobic mesoporous silica, here, the Langmuir function fits better if using χ^2 as measure for non-linear fits (lower χ^2 indicates a better fit, χ^2 = 1.36 for the Langmuir fit, dashed line in Figure 8B, compared to χ^2 = 4.20 for the Freundlich fit, solid line in Figure 8B).[42] As compared to the rather unspecific adsorption of hydrocarbons into hydrophobic

mesoporous silica films that allowed for multilayer adsorption (according to the Freundlich model), the trimethylammonium functionalized films offered just one binding site per nitrate ion. This is in accordance with the definition of Langmuir adsorption isotherms and previously reported batch experiments.[13,43] The derived Langmuir function served as calibration function. This allowed for retrieving the limit of detection (LOD) defined as q_e(LOD)= 3·σ, with σ being the standard deviation derived from 100 % lines obtained from consecutive blank water spectra. This yielded a LOD of 1.2 mg L^{-1} for the presented ATR-IR filtometer.

According to quantitative considerations performed in section 3.1.2, the enriched amount of NO_3^- per volume was also derived from these experiments. The band area obtained from a 7.3 mg L^{-1} NO_3^- solution corresponds to a concentration of 11.7 g L^{-1}_{film}, which is equivalent to a trimethylammonium moiety consumption of 14 % and an enrichment factor of 1600. The threefold enrichment factor compared to FTIR measurements is in accordance with the loss of the trimethylammonium moieties as determined from IR spectra of the as-synthesized film compared to the aged film. The maximum adsorption capacity obtained from the Langmuir fit q_m was calculated to be 10.4 A.U.·cm^{-1} (equal to $q_{m,mass} = q_m /(\varepsilon \cdot d_{e,film})$ =26.1 g_{NO3-} L^{-1}_{film}), which corresponds to trimethylammonium moiety consumption of 32 %. The anion exchange reactions can be described as an equilibrium between different monovalent anions present in solution. Therefore, the incomplete consumption of the trimethylammonium moiety can be attributed to the adjustment of equilibrium between NO_3^- and OH^-, as reported for other anion pairs on similar materials.[44]Nitrate enrichment experiments reported in literature have been performed using powdered mesoporous materials for enrichment from batch solutions. [13,43] In these reports the achieved enrichment is generally expressed as absorbed amount of analyte per employed amount of silica, $mg_{Analyte}$ g_{SiO2}^{-1}. In order to compare our results with these literature data, the retrieved concentrations in g_{NO3-} L^{-1}_{film} were expressed in these terms. The film density of ρ=1.32 g cm^{-3} was calculated as the weighted averaged density from the density of bulk silica with a film porosity of 50 %.[45] With this, a maximum absorption capacity of 20 mg_{NO3-} g_{SiO2}^{-1} (derived from $q_{m,mass/}$ ρ) was obtained, which is in similar to ~30 mg_{NO3-} g_{SiO2}^{-1} obtained for batch experiments after 1 h of equilibration time for similar materials[13,43] and in the range of commercially available anion exchange resins.[46]

4. Conclusion and Outlook

A multibounce ATR crystal was combined with a FP filter and a miniaturized mid-IR emitter in a 3D-printed ATR-IR filtometer. The ATR crystal was coated with mesoporous silica films functionalized with a trimethylammonium ion exchange moiety allowing for nitrate enrichment. The films were characterized using a FTIR spectrometer and showed response times of a few seconds and full recovery upon rinsing

with diluted HCl. Using the ATR-IR filtometer aqueous nitrate solutions with concentrations between 3.6 mg L^{-1} to 70 mg L^{-1} were measured. The obtained data were fitted with the Langmuir equation that served as calibration function and allowed for retrieving a limit of detection of 1.2 mg L^{-1}. The steep slope of the Langmuir function up to a concentration of 40 mg L^{-1} nitrate in water enabled sensitive measurements of nitrate concentrations at drinking water levels. Although only a third of the present trimethylammonium groups in the film interacted with nitrate ions, high enrichment factors of up to 1600 were determined. It was found that nitrate enrichment was not possible in the presence of multiply charged sulfate ions. To overcome this, established knowledge of silica surface tuning routinely used for chromatography columns materials could be transferred and utilized also for ATR spectroscopy-based sensing. For instance, the affinity of the ion exchange group towards multiply charged ions could be decreased by using an ammonium moiety with *n*-butyl groups instead of methyl groups.[47–49] Due to the higher steric hindrance of the butyl groups the ammonium cation would be less accessible to larger ions. Furthermore, cations could be targeted by introducing a sulfonic acid moiety into the film. In summary, the rich surface chemistry of silica in combination with the presented pocket-sized, cost effective ATR-IR filtometer, which could be operated using a battery due to its low power consumption, resembles a promising candidate for portable drinking water sensors.

AUTHOR INFORMATION

Corresponding Author

*Email: bernhard.lendl@tuwien.ac.at

Author Contributions

All authors have given approval to the final version of the manuscript.

ACKNOWLEDGMENTS

This work is part of the AQUARIUS and WATERSPY project, which have received funding from the European Union's Horizon 2020 research and innovation program under grant agreement No. 731465 and 731778. These projects are an initiative of the Photonics Public Private Partnership. IMEC is acknowledged for providing Ge samples.

References

1. World Health Organization. *Guidelines for Drinking-water Quality*. **1**, (2017).
2. Ward, M. H., Jones, R. R., Brender, J. D., de Kok, T. M., Weyer, P. J., Nolan, B. T., Villanueva, C. M.

& van Breda, S. G. Drinking water nitrate and human health: An updated review. *International Journal of Environmental Research and Public Health* **15**, (2018).

3. Laue, W., Thiemann, M., Scheibler, E. & Wiegand, K. W. Nitrates and Nitrites. in *Ullmann's Encyclopedia of Industrial Chemistry* (Wiley-VCH Verlag GmbH & Co. KGaA, 2000). doi:10.1002/14356007.a17_265
4. Patton, C. J. & Kryskalla, J. R. Analytical Properties of Some Commercially Available Nitrate Reductase Enzymes Evaluated as Replacements for Cadmium in Automated , Semiautomated , and Manual Colorimetric Methods for Determination of Nitrate Plus Nitrite in Water Model of Nitrate Reducta. *Sci. Investig. Rep. 2013–5033* (2013).
5. Huebsch, M., Grimmeisen, F., Zemann, M., Fenton, O., Richards, K. G., Jordan, P., Sawarieh, A., Blum, P. & Goldscheider, N. Technical Note: Field experiences using UV/VIS sensors for high-resolution monitoring of nitrate in groundwater. *Hydrol. Earth Syst. Sci.* **19**, 1589–1598 (2015).
6. Langergraber, G., Fleischmann, N. & Hofstädter, F. A multivariate calibration procedure for UV/VIS spectrometric quantification of organic matter and nitrate in wastewater. in *Water Science and Technology* **47**, 63–71 (IWA Publishing, 2003).
7. Rieger, L., Langergraber, G., Thomann, M., Fleischmann, N. & Siegrist, H. Spectral in-situ analysis of NO2, NO3, COD, DOC and TSS in the effluent of a WWTP. *Water Sci. Technol.* **50**, 143–152 (2004).
8. Ramer, G. & Lendl, B. Attenuated Total Reflection Fourier Transform Infrared Spectroscopy. in *Encyclopedia of Analytical Chemistry* (John Wiley & Sons, Ltd, 2013).
9. Dobbs, G. T., Balu, B., Young, C., Kranz, C., Hess, D. W. & Mizaikoff, B. Mid-Infrared Chemical Sensors Utilizing Plasma-Deposited Fluorocarbon Membranes. **79**, 9566–9571 (2007).
10. Lu, R., Mizaikoff, B., Li, W.-W., Qian, C., Katzir, A., Raichlin, Y., Sheng, G.-P. & Yu, H.-Q. Determination of Chlorinated Hydrocarbons in Water Using Highly Sensitive Mid-Infrared Sensor Technology. *Sci. Rep.* **3**, 1–6 (2013).
11. Lu, Y., Han, L., Brinker, C. J., Niemczyk, T. M. & Lopez, G. P. Chemical sensors based on hydrophobic porous sol-gel films and ATR-FTIR spectroscopy. *Sensors Actuators B Chem.* **36**, 517–521 (1996).
12. Baumgartner, B., Hayden, J., Schwaighofer, A. & Lendl, B. In Situ IR Spectroscopy of Mesoporous Silica Films for Monitoring Adsorption Processes and Trace Analysis. *ACS Appl. Nano Mater.* **1**, 7083–7091 (2018).
13. Dioum, A. & Hamoudi, S. Mono- and quaternary-ammonium functionalized mesoporous silica materials for nitrate adsorptive removal from water and wastewaters. *J. Porous Mater.* **21**, 685–690 (2014).
14. Saad, R., Hamoudi, S. & Belkacemi, K. Adsorption of phosphate and nitrate anions on ammonium-functionnalized mesoporous silicas. *J. Porous Mater.* **15**, 315–323 (2008).
15. Vermeir, S., Beullens, K., Mészáros, P., Polshin, E., Nicolaï, B. M. & Lammertyn, J. Sequential injection ATR-FTIR spectroscopy for taste analysis in tomato. *Sensors Actuators, B Chem.* **137**, 715–721 (2009).
16. Freitag, S., Baumgartner, B., Tauber, S., Gasser, C., Radel, S., Schwaighofer, A. & Lendl, B. An Acoustic Trap for Bead Injection Attenuated Total Reflection Infrared Spectroscopy. *Anal. Chem.* **91**, 7672–7678 (2019).
17. Hinsmann, P., Haberkorn, M., Frank, J., Svasek, P., Harasek, M. & Lendl, B. Time-resolved FT-IR spectroscopy of chemical reactions in solution by fast diffusion-based mixing in a micromachined flow cell. *Appl. Spectrosc.* **55**, 241–251 (2001).
18. Jarute, G., Kainz, A., Schroll, G., Baena, J. R. & Lendl, B. On-line determination of the intracellular poly(β-hydroxybutyric acid) content in transformed Escherichia coli and glucose during PHB production using stopped-flow attenuated total reflection FT-IR spectrometry. *Anal. Chem.* **76**, 6353–6358 (2004).
19. Koch, C., Brandstetter, M., Wechselberger, P., Lorantfy, B., Plata, M. R., Radel, S., Herwig, C. &

Lendl, B. Ultrasound-enhanced attenuated total reflection mid-infrared spectroscopy in-line probe: Acquisition of cell spectra in a bioreactor. *Anal. Chem.* **87**, 2314–2320 (2015).
20. Lumpi, D., Wagner, C., Schöpf, M., Horkel, E., Ramer, G., Lendl, B. & Fröhlich, J. Fibre optic ATR-IR spectroscopy at cryogenic temperatures: In-line reaction monitoring on organolithium compounds. *Chem. Commun.* **48**, 2451–2453 (2012).
21. Baumgartner, B., Hayden, J., Loizillon, J., Steinbacher, S., Grosso, D. & Lendl, B. Pore Size-Dependent Structure of Confined Water in Mesoporous Silica Films from Water Adsorption/Desorption Using ATR–FTIR Spectroscopy. *Langmuir* **35**, 11986–11994 (2019).
22. Nabers, A., Ollesch, J., Schartner, J., Kötting, C., Genius, J., Haußmann, U., Klafki, H., Wiltfang, J. & Gerwert, K. An infrared sensor analysing label-free the secondary structure of the Abeta peptide in presence of complex fluids. *J. Biophotonics* **9**, 224–234 (2016).
23. Bürgi, T. & Baiker, A. Attenuated Total Reflection Infrared Spectroscopy of Solid Catalysts Functioning in the Presence of Liquid-Phase Reactants. *Adv. Catal.* **50**, 227–283 (2006).
24. Finlayson, D., Rinaldi, C. & Baker, M. J. Is Infrared Spectroscopy Ready for the Clinic? *Anal. Chem.* **91**, 12117–12128 (2019).
25. Wilks, P. Infrared Filtometers. in *Handbook of Vibrational Spectroscopy* (eds. Chalmers, J. M. & Griffiths, P. R.) (J. Wiley, 2006). doi:10.1002/0470027320.s0203
26. Jerman, J. H., Clift, D. J. & Mallinson, S. R. A miniature Fabry-Perot interferometer with a corrugated silicon diaphragm support. *Sensors Actuators A. Phys.* **29**, 151–158 (1991).
27. InfraTec. Durchstimmbare Detektoren (FPI Detektor) von InfraTec. Available at: https://www.infratec.at/sensorik/fpi-detektoren/. (Accessed: 13th September 2019)
28. Neumann, N., Ebermann, M., Hiller, K. & Kurth, S. Tunable infrared detector with integrated micromachined Fabry-Perot filter. in *MOEMS and Miniaturized Systems VI* (eds. Dickensheets, D. L., Gogoi, B. P. & Schenk, H.) **6466**, 646606 (International Society for Optics and Photonics, 2007).
29. Kurth, S., Hiller, K., Neumann, N., Heinze, M., Doetzel, W. & Gessner, T. Tunable Fabry-Perot-Interferometer for 3-5 µm wavelength with bulk micromachined reflector carrier. in *SPIE 4983, MOEMS and Miniaturized Systems III* (ed. Smith, J. H.) **4983**, 215 (International Society for Optics and Photonics, 2003).
30. Genner, A., Gasser, C., Moser, H., Ofner, J., Schreiber, J. & Lendl, B. On-line monitoring of methanol and methyl formate in the exhaust gas of an industrial formaldehyde production plant by a mid-IR gas sensor based on tunable Fabry-Pérot filter technology. *Anal. Bioanal. Chem.* **409**, 753–761 (2017).
31. Gasser, C., Genner, A., Moser, H., Ofner, J. & Lendl, B. Application of a tunable Fabry-Pérot filtometer to mid-infrared gas sensing. *Sensors Actuators, B Chem.* **242**, 9–14 (2017).
32. Kilgus, J., Duswald, K., Langer, G. & Brandstetter, M. Mid-Infrared Standoff Spectroscopy Using a Supercontinuum Laser with Compact Fabry–Pérot Filter Spectrometers. *Appl. Spectrosc.* **72**, 634–642 (2018).
33. Gasser, C., Kilgus, J., Harasek, M., Lendl, B. & Brandstetter, M. Enhanced mid-infrared multi-bounce ATR spectroscopy for online detection of hydrogen peroxide using a supercontinuum laser. *Opt. Express* **26**, 12169 (2018).
34. Gattinger, P., Kilgus, J., Zorin, I., Langer, G., Nikzad-Langerodi, R., Rankl, C., Gröschl, M. & Brandstetter, M. Broadband near-infrared hyperspectral single pixel imaging for chemical characterization. *Opt. Express* **27**, 12666 (2019).
35. Kischkat, J., Peters, S., Gruska, B., Semtsiv, M., Chashnikova, M., Klinkmüller, M., Fedosenko, O., Machulik, S., Aleksandrova, A., Monastyrskyi, G., Flores, Y. & Ted Masselink, W. Mid-Infrared Optical Properties of Thin Films of Aluminum Oxide, Titanium Dioxide, Silicon Dioxide, Aluminum Nitride, and Silicon Nitride. *Appl. Opt.* **51**, 6789–6798 (2012).
36. Hale, G. M. & Querry, M. R. Optical Constants of Water in the 200-nm to 200-µm Wavelength

Region. *Appl. Opt.* **12**, 555 (1973).
37. Brinker, J. C., Lu, Y., Sellinger, A. & Fan, H. Evaporation-Induced Self-Assembly: Nanostructures Made Easy. *Adv. Mater.* **11**, 579–585 (1999).
38. Grosso, D., Cagnol, F., Soler-Illia, G. J. D. A. A., Crepaldi, E. L., Amenitsch, H., Brunet-Bruneau, A., Bourgeois, A. & Sanchez, C. Fundamentals of mesostructuring through evaporation-induced self-assembly. *Adv. Funct. Mater.* **14**, 309–322 (2004).
39. Carteret, C. Mid- and near-infrared study of hydroxyl Groups at a silica surface: H-Bond effect. *J. Phys. Chem. C* **113**, 13300–13308 (2009).
40. Vonach, R., Lendl, B. & Kellner, R. Modulation of the pH in the determination of phosphate with flow injection and Fourier transform infrared detection. *Analyst* **122**, 525–530 (1997).
41. Schwaighofer, A., Alcaraz, M. R., Lux, L. & Lendl, B. pH titration of β-lactoglobulin monitored by laser-based Mid-IR transmission spectroscopy coupled to chemometric analysis. *Spectrochim. Acta Part A Mol. Biomol. Spectrosc.* **226**, 117636 (2019).
42. Ho, Y. S. Selection of Optimum Sorption Isotherm. *Carbon N. Y.* **42**, 2115–2116 (2004).
43. Hamoudi, S. & Belkacemi, K. Adsorption of nitrate and phosphate ions from aqueous solutions using organically-functionalized silica materials: Kinetic modeling. *Fuel* **110**, 107–113 (2013).
44. De Campos, E. A., Da Silva Alfaya, A. A., Ferrari, R. T. & Costa, C. M. M. Quaternary ammonium salts immobilized on silica gel: Exchange properties and application as potentiometric sensor for perchlorate ions. *J. Colloid Interface Sci.* **240**, 97–104 (2001).
45. Baumgartner, B., Hayden, J., Loizillon, J., Steinbacher, S., Grosso, D. & Lendl, B. Pore Size-Dependent Structure of Confined Water in Mesoporous Silica Films from Water Adsorption-Desorption using ATR-FTIR Spectroscopy. *Langmuir* (2019). doi:10.1021/acs.langmuir.9b01435
46. Sowmya, A. & Meenakshi, S. Removal of nitrate and phosphate anions from aqueous solutions using strong base anion exchange resin. *Desalin. Water Treat.* **51**, 7145–7156 (2013).
47. Guter, G. A. Removal of nitrate from water supplies using a tributyl amine strong base anion exchange resin. (1983).
48. McGarvey, F. X. & Gonzalez, R. Ion Exchange Studies on Strongly Basic Anion Exchange Resins Prepared with Tertiary Amines of Varying Molecular Weight. in *Ion Exchange Advances* 97–103 (Springer Netherlands, 1992). doi:10.1007/978-94-011-2864-3_13
49. Sata, T., Yamaguchi, T. & Matsusaki, K. Effect of hydrophobicity of ion exchange groups of anion exchange membranes on permselectivity between two anions. *J. Phys. Chem.* **99**, 12875–12882 (1995).